THE ASTROPHYSICAL JOURNAL, 359:363–377, 1990 August 20

OPTICAL POLARIZATION MAPS OF STAR-FORMING REGIONS IN PERSEUS, TAURUS, AND OPHIUCHUS

A. A. GOODMAN,[1,2] P. BASTIEN,[3] P. C. MYERS,[1] AND F. MÉNARD[3]

Received 1989 October 23; accepted 1990 February 9

ABSTRACT

We present new optical linear polarization maps of the star-forming regions near L1506 in Taurus, L1755 in Ophiuchus, and the complex of dark clouds which extends from L1448 to B5 in Perseus. In the L1506 region, the polarization vectors show a systematic alignment with each other but are oriented at about 25° to the projected axis of the local dark cloud. This pattern fits in smoothly with a large-scale polarization map of the Taurus cloud complex. In the L1755 region, the individual polarization vectors are remarkably well aligned with each other and with the projected elongation of the cloud. As in Taurus, this observed alignment may be understood in view of a polarization map of the entire Ophiuchus cloud complex. In Perseus, no simple pattern can be discerned: the distribution of polarization vector orientation appears bimodal, with small vectors parallel to the overall projected cloud axis and larger vectors perpendicular. We propose that this bimodal distribution is due to polarization produced by magnetically aligned grains which are located in more than one cloud complex along the line of sight of Perseus. Molecular spectral line observations, which show gas in two distinct velocity ranges, support this hypothesis.

The distributions of polarization vector angle, θ, can be decomposed into a peak direction, a dispersion about that peak, and a random component. We model the peak and its dispersion as arising from a uniform field with nonuniform perturbations about it.

The dispersion in θ for an entire cloud complex is generally less than the variations in position angle of the long axis of filamentary clouds (observed in extinction or molecular lines) within the complex, suggesting that the magnetic field does not dominate the cloud structure on the size scale $\gtrsim 1$ pc.

Subject headings: interstellar: magnetic fields — interstellar: matter — nebulae: general — polarization

I. INTRODUCTION

The magnetic field strength and direction are important parameters in the physics of molecular clouds. In clouds noticeable as dark patches of extinction on optical photographs ("dark clouds"), where the density of H_2 molecules, n, is $\gtrsim 10^2$–10^3 cm^{-3}, we can measure line-of-sight strength with radio frequency Zeeman observations, and we can map the field morphology in the plane of the sky with optical polarization observations.

Magnetic field strengths derived from Zeeman work are consistent with approximate equality between magnetic, gravitational, and kinetic energy in molecular clouds over a density range $10 \lesssim n \lesssim 10^8$ cm^{-3} (see Myers and Goodman 1988*a*, and references therein). The fact that the Zeeman effect, which is sensitive only to line-of-sight magnetic field,[4] is detected at all implies that there is a significant uniform component of the magnetic field in molecular clouds. The similarity between the field strengths measured by Zeeman observations and the field strength derived from "equilibrium" models further implies approximate equality between the uniform component of the field and the equilibrium field.

To gain a more detailed understanding of the magnetic field distribution, we measured the linear polarization of stars background to three molecular cloud regions: L1506 in Taurus, L1755 in Ophiuchus, and the complex of dark clouds which extends from L1448 to B5 in Perseus.

The polarization we observe is generally believed to arise from selective extinction by nonspherical dust grains aligned by interstellar magnetic fields. The detailed process(es) by which grains become aligned with magnetic fields has long been (e.g., Davis and Greenstein 1951), and is still (e.g., Dolginov 1990), actively under study. In general, over long time scales ($\sim 10^6$ yr in a dark cloud), grains tend to become aligned with their shortest axis parallel to the magnetic field (Purcell 1979). Therefore, the amount of extinction caused by the aligned grains is greatest along the direction parallel to the plane-of-the-sky projection of their longest axis. And, the transmission maximum (the observed position angle of linear polarization) is parallel to the plane-of-the-sky projection of the magnetic field.

Previous polarization maps of elongated molecular clouds have shown that various configurations of the plane-of-the-sky magnetic field, $\boldsymbol{B}_\perp$, with respect to the projected shape of the clouds are observed. In some clouds, the polarization vectors are roughly perpendicular to the projected cloud elongation (e.g., B216/217 [Heyer *et al.* 1987], Lupus 1 [see Strom, Strom, and Edwards 1988], or L204 [McCutcheon *et al.* 1986]). In other, similar, clouds, it is claimed, on the basis of polarization maps, that $\boldsymbol{B}_\perp$ is (roughly) parallel to the projected cloud elongation (e.g., the B42 cloud in Ophiuchus [Vrba, Strom, and Strom 1976], the eastern part of the R CrA cloud [Vrba, Coyne, and Tapia 1981], the globular filament GF 7 in Cygnus [McDavid 1984], or L1641 [Vrba, Strom and Strom 1988]), although the maps and the authors admit a large amount of scatter about the mean. And, in the remaining cases where

[1] Harvard-Smithsonian Center for Astrophysics.
[2] Department of Physics, Harvard University.
[3] Observatoire du Mont Mégantic and Département de Physique, Université de Montréal.

[4] In cases where the Zeeman splitting is much less than the observed spectral line width, which includes all nonmasing regions, to date.

polarization maps of elongated clouds have been made, the field is neither "perpendicular" nor "parallel" to the projected cloud axis, e.g., B18 (Heyer *et al.* 1987).

In fact, "parallel" and "perpendicular" are not well-defined terms when evaluating the relationship between polarization vectors and cloud shapes. In the above examples, some of which are cited as examples of "magnetically dominated clouds," owing to the "parallel" or "perpendicular" orientation of the *projected* cloud axis with respect to the *plane-of-the-sky* magnetic field, there is a non-negligible difference (e.g., 30°) between the cloud axis and the direction parallel (or perpendicular) to the average polarization observed, and there is a large scatter, typically $20° \simeq 30°$ about this average. Therefore, it is important to assemble a large sample of polarization observations, and to assess "alignments" quantitatively, with attention to the projection of three-dimensional orientations into the two-dimensional plane of the sky.

It was the goal of our observations to add to the growing, but still small, sample of optical polarization maps of background starlight, in order to better understand the (projected) magnetic field geometry in regions of star formation.

Our main conclusion is that, in most cloud complexes, there is a smooth pattern in the large-scale polarization maps—average polarization vector angles vary only slightly across the complex, but the orientation of elongated individual clouds within a complex varies more. If the polarization vectors are truly representative of the large-scale magnetic field, this result implies that cloud structural features are not necessarily aligned with the magnetic field, even though the field may be energetically significant.

We discuss the method used to measure optical polarization in § II. In § III, we present and discuss the results obtained in L1506, L1755, and Perseus. Section IV presents the results of Gaussian fits to the large-scale distributions of polarization vector angle in Taurus, Ophiuchus, and Perseus. In § V, we discuss our results, in general, and in the context of previous observations. We summarize the paper and suggest future investigations in the concluding § VI.

II. OBSERVATIONS

The observations were carried out at the Mont Mégantic Observatory[5] on a 1.6 m Ritchey-Chrétien telescope fitted with a two-channel photoelectric polarimeter similar to that described by Angel and Landstreet (1970). The observations of L1506, L1755, and Perseus were carried out in 1987 November, 1988 June, and 1988 November/December, respectively. We used a Schott RG-645 filter which gives a broad passband of 2450 Å, centered at 7625 Å. A small instrumental polarization (~0.05%–0.1%, depending on the observing season) was accurately determined and subtracted from the observations; the observational errors were adjusted accordingly. The polarization scale was determined with a Glan prism which gives essentially 100% polarized light. The origin of the position angles was determined by observing standard polarized stars. Most of these standards have been found recently to be variable at a small scale (Bastien *et al.* 1988), but since more than one star was used, we expect this (constant for any one observing period) calibration error to be of the order of 1° or less. For each star observed, we used an integration time sufficient to reduce the random (1 σ) uncertainty in its polarization (due to instrumental sensitivity limitations and photon statistics) to ~0.1%.

The particular stars observed in a cloud were selected from the Palomar Sky Survey E-plates by virtue of their being coincident, in projection, with the periphery of the extinction associated with dark clouds. We attempted to exclude foreground stars by not selecting stars which appear relatively bright but are isolated in regions of otherwise high extinction. We believe nearly all the stars selected in this way are background to the cloud of interest, since all the clouds are relatively close, with distances: Taurus ~140 pc (Elias 1978); Ophiuchus ~160 pc (Bertiau 1958); and Perseus[6] ~350 pc (Herbig and Jones 1983).

III. RESULTS AND DISCUSSION OF INDIVIDUAL CLOUDS

a) L1506 and Taurus

The polarization data for the L1506 cloud are listed in Table 1, and they are superposed on an optical photograph of the region in Figure 1. L1506 is clearly visible in the photograph as a well-defined dark lane of extinction, about 4 pc × 0.6 pc in size[7]. Figure 2*a* shows a broad peak in the distribution of percent linear polarization (P) for the stars associated in projection with this cloud, with a mean of 1.6%, and a standard deviation of 0.7%. Figure 2*b* shows a peak in the distribution of polarization vector angle (θ, measured east of north) centered at a mean of 82°, with a standard deviation of 26°.[8] The position angle of the cloud,[9] as projected on the sky, is 105° E of N, or about 23° from the peak of the observed polarization vector angle. The plane parallel to the galactic plane at the cloud's galactic latitude, $b = -17°$, projects in this region to a direction 140° E of N, not related, in an obvious way at this size scale, to the distribution of θ observed.

To put our L1506 observations into the perspective of the Taurus molecular cloud complex, we have plotted the data listed in Table 1 along with the extensive Moneti *et al.* (1984) polarization observations, and the Heyer *et al.* (1987) detailed polarization observations of the clouds near B216/B217 and B18 (Fig. 3). The pattern of polarization vectors observed in Taurus is smooth, and the average local position angle of the polarization vectors varies slowly with position, by about 30° over a projected distance of 20 pc.[10]

[5] The Mont Mégantic Observatory is operated by the Université de Montréal and Laval University, Québec, Canada.

[6] See § IV*b* for further discussion of the distance to the Perseus cloud complex.

[7] The western end of L1529 (a.k.a., B18), a similar dark cloud where Heyer *et al.* (1987) have constructed optical polarization maps, lies less than 30′ (1.2 pc) from the eastern end of the L1506 cloud, and it is not shown in Fig. 1.

[8] Throughout the text, the terms "mean" and "standard deviation" refer to an unweighted mean and the rms deviation about that mean. We have also calculated means weighted by the uncertainty in each value, but since the number of cases with large errors is very small compared to the total number of cases the weighted means are consistent, within errors, with the unweighted means. A third method for calculating the mean P and θ would be to treat all vectors as if they were repeated measurements of the same quantity (see Bastien 1982*a*, *b*), which would tell us what polarization we would observe if our aperture included all the background stars at once. This last method can provide useful information about the uniformity of the field, but it does not characterize the "typical" value of P if θ varies significantly among the measurements.

[9] Measured by fitting a straight line through the positions of all stars observed, which were selected to trace the outline of the cloud.

[10] A note about a smaller scale: Tamura *et al.* (1987) have constructed a 2.2 μm polarization map of 14 background stars in the immediate vicinity (~2 pc radius) of TMC-1, in Heiles Cloud 2 (centered near 04^h37^m; 25°40′). The pattern they observe is consistent with the large-scale field orientation depicted in Fig. 3.

TABLE 1

L1506 POLARIMETRY

Star	R.A. (1950)	Decl. (1950)	P (%)	$\epsilon(P)$ (%)	θ (E of N)	$\epsilon(\theta)$
1.....	$4^h15^m08^s$	25°12′39″	1.90	0.11	126°	2°
2.....	4 15 18	25 17 08	2.16	0.17	107	2
3.....	4 15 23	25 02 26	1.62	0.12	80	2
4.....	5 15 38	25 20 31	1.99	0.10	93	1
5.....	4 15 49	25 07 03	2.20	0.09	86	1
6.....	4 16 01	25 22 11	2.26	0.10	79	1
7.....	4 16 18	25 04 29	2.02	0.08	79	1
8.....	4 16 59	25 15 34	1.75	0.26	82	4
9.....	4 17 02	25 02 52	1.18	0.09	61	2
10.....	4 17 10	25 10 41	0.12	0.12	158	28
11.....	4 17 18	25 20 44	1.42	0.11	75	2
12.....	4 17 23	25 15 14	0.87	0.16	115	5
13.....	4 17 28	25 01 54	1.24	0.08	61	2
14.....	4 17 52	24 52 36	1.76	0.10	62	2
15.....	4 17 52	25 02 45	0.99	0.10	70	3
16.....	4 17 55	25 14 19	0.52	0.11	80	6
17.....	4 18 03	25 06 08	2.44	0.15	93	2
18.....	4 18 26	25 13 53	0.93	0.11	85	3
19.....	4 18 29	24 58 44	1.37	0.18	7	4
20.....	4 18 46	24 54 57	1.83	0.11	76	2
21.....	4 18 52	25 09 32	1.31	0.09	82	2
22.....	4 19 03	24 55 17	1.71	0.12	82	2
23.....	4 19 03	24 55 20	0.17	0.13	128	21
24.....	4 19 07	25 07 10	0.65	0.12	66	5
25.....	4 19 14	25 12 42	0.89	0.10	57	3
26.....	4 19 42	24 50 01	1.60	0.10	83	2
27.....	4 19 47	25 04 25	2.10	0.06	99	1
28.....	4 20 04	25 01 32	0.07	0.06	115	23
29.....	4 20 14	25 08 52	1.95	0.07	68	1
30.....	4 20 20	24 46 59	1.61	0.12	102	2
31.....	4 20 34	24 48 19	3.40	0.09	86	1
32.....	4 20 37	24 49 14	1.28	0.13	124	3
33.....	4 20 41	25 06 00	1.93	0.10	62	1
34.....	4 20 54	24 45 23	2.34	0.12	72	1
35.....	4 20 58	25 04 32	1.65	0.11	57	2
36.....	4 21 24	24 41 37	1.80	0.09	62	1
37.....	4 21 25	24 58 35	2.02	0.09	59	1
38.....	4 21 35	24 55 05	2.42	0.14	60	2
39.....	4 21 40	24 47 43	1.63	0.23	74	4
40.....	4 21 41	24 40 58	1.82	0.13	65	2
Mean			1.57	0.11	82	4
Standard Deviation			0.68	0.04	26	6

NOTE.—The uncertainty in θ is given by the formula $\epsilon(\theta) = 28.^\circ65\ [\epsilon(P)/P]$ in cases where the uncertainty in P, $\epsilon(P) \ll P$, and $\epsilon(\theta) = 51.^\circ96$ otherwise (Serkowski 1974).

Figure 3 gives the best "picture" of the plane-of-the-sky magnetic field in Taurus. From a quantitative point of view, though, we can sacrifice the large amount of spatial information in the map and analyze the overall distribution of P and θ in the region (Figs. 4*a* and 4*b*). The mean percentage polarization, which corresponds well to the peak of the distribution (Fig. 4*a*) is 2.1%, with a standard deviation of 1.4%. The mean of θ, which also corresponds to the peak in the distribution (Fig. 4*b*) is 54°, with a standard deviation of 33°. This distribution of position angle is analyzed further in § IV*a*.

b) L1755 and Ophiuchus

On an optical photograph of the region near L1755 in Ophiuchus (Fig. 5), the cloud is clearly visible as a well-defined dark lane of extinction, about 6 pc × 0.7 pc in size. The polarization data for the L1755 cloud are listed in Table 2, and they are superposed on contours of ^{13}CO intensity (Loren 1989*a*) in Figure 6. As is clearly evident in Figure 6, the polarization vectors in L1755 are remarkably well aligned with each other and with the cloud's projected long axis.

Figure 7*a* shows a clear peak in the distribution of P for the stars associated in projection with this cloud, with a mean of 4.2%, and a standard deviation of 1.5%. Figure 7*b* shows a very sharp (as one would expect from the map) peak in the distribution of θ centered at a mean of 61°, with a standard

TABLE 2

L1755 POLARIMETRY

Star	R.A. (1950)	Decl. (1950)	P (%)	$\epsilon(P)$ (%)	θ (E of N)	$\epsilon(\theta)$
1.....	$16^h35^m55^s$	−22°23′06″	4.29	0.10	60°	1°
2.....	16 35 57	−22 16 08	6.26	0.17	55	1
3.....	16 36 12	−22 23 15	3.33	0.11	63	1
4.....	16 36 27	−22 16 19	4.46	0.11	56	1
5.....	16 36 44	−22 12 06	0.07	0.10	4	38
6.....	16 36 57	−22 25 03	2.71	0.11	57	1
7.....	16 37 35	−22 19 46	2.51	0.12	64	1
8.....	16 38 14	−22 15 42	1.62	0.11	73	2
9.....	16 38 18	−22 22 25	1.59	0.12	90	2
10.....	16 38 38	−22 08 32	5.33	0.10	53	1
11.....	16 38 58	−21 58 45	5.87	0.12	48	1
12.....	16 39 07	−22 17 02	3.89	0.09	70	1
13.....	16 39 16	−21 59 28	4.50	0.14	53	1
14.....	16 39 16	−21 44 27	6.02	0.13	59	1
15.....	16 39 25	−22 13 31	3.75	0.14	70	1
16.....	16 39 38	−22 10 04	4.33	0.10	71	1
17.....	16 39 58	−22 07 56	4.21	0.10	73	1
18.....	16 39 58	−21 53 44	4.22	0.11	49	1
19.....	16 40 01	−21 40 42	0.13	0.10	162	21
20.....	16 40 15	−21 53 42	3.64	0.13	47	1
21.....	16 40 27	−21 31 42	4.92	0.10	51	1
22.....	16 40 28	−21 45 48	4.25	0.13	43	1
23.....	16 40 34	−22 01 27	4.41	0.10	73	1
24.....	16 40 55	−21 26 00	3.65	0.10	52	1
25.....	16 41 18	−22 01 17	2.88	0.10	80	1
26.....	16 41 26	−21 51 16	0.19	0.10	178	16
27.....	16 41 35	−21 31 07	5.21	0.13	45	1
28.....	16 41 53	−21 12 54	3.38	0.12	20	1
29.....	16 41 54	−21 19 36	4.58	0.11	35	1
30.....	16 41 56	−21 39 08	4.85	0.26	61	2
31.....	16 42 13	−21 01 13	3.82	0.10	38	1
32.....	16 42 15	−21 11 16	5.38	0.14	27	1
33.....	16 42 38	−21 36 52	5.16	0.10	54	1
34.....	16 42 49	−21 36 11	6.10	0.09	61	1
35.....	16 42 53	−21 20 27	4.30	0.13	57	1
36.....	16 42 56	−21 07 01	4.88	0.11	49	1
37.....	16 42 59	−21 28 22	6.30	0.18	57	1
38.....	16 43 15	−21 23 05	7.48	0.12	58	1
39.....	16 43 19	−20 59 51	3.17	0.20	66	2
40.....	16 43 45	−21 29 30	5.24	0.10	64	1
41.....	16 44 17	−20 58 22	4.34	0.10	45	1
42.....	16 44 19	−21 20 09	4.89	0.15	60	1
43.....	16 44 19	−21 08 25	4.95	0.12	62	1
44.....	16 44 21	−21 30 20	4.66	0.12	60	1
45.....	16 44 22	−21 02 27	3.88	0.14	44	1
46.....	16 44 27	−21 29 35	4.98	0.10	62	1
47.....	16 44 37	−21 15 54	4.23	0.10	64	1
48.....	16 44 49	−21 16 02	4.49	0.10	60	1
49.....	16 44 57	−21 30 17	4.08	0.14	56	1
50.....	16 45 10	−21 15 58	4.33	0.10	65	1
51.....	16 45 15	−21 19 39	4.23	0.03	65	1
Mean			4.16	0.12	61	2
Standard Deviation			1.48	0.03	26	6

NOTE.—The uncertainty in θ is given by the formula $\epsilon(\theta) = 28.^\circ65\ [\epsilon(P)/P]$ in cases where the uncertainty in P, $\epsilon(P) \ll P$, and $\epsilon(\theta) = 51.^\circ96$ otherwise (Serkowski 1974).

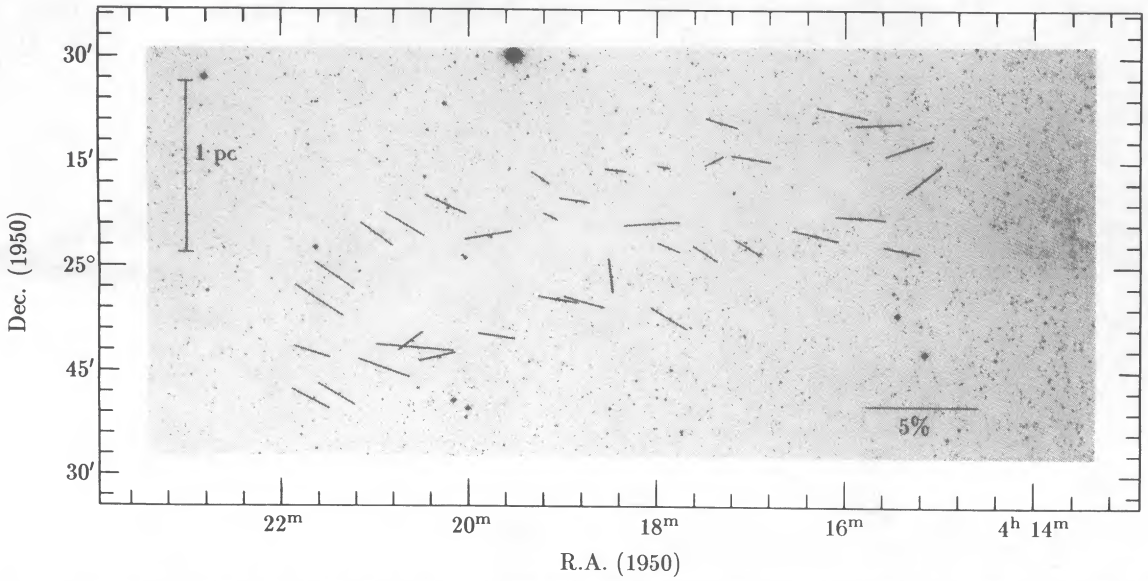

FIG. 1.—An optical polarization map of the L1506 dark cloud in Taurus, superposed on a reproduction of the Palomar Sky Survey E-plate. The length of the vectors is proportional to the percentage linear polarization at the illustrated position angle.

deviation of 26°. The position angle of the cloud,[11] as projected on the sky, is 61° E of N, identical to the mean in the observed polarization vector angle. The plane parallel to the galactic plane at the cloud's galactic latitude, $b = 15°$, projects in this region to a direction of 25° E of N, not related, in an obvious way at this size scale, to the distribution of θ observed.

When the L1755 data are put in context with the existing polarization measurements (Vrba, Strom, and Strom 1976; Wilking *et al.* 1979)[12] in Ophiuchus (see Fig. 8), it becomes apparent that there is a well-defined average field direction in the region, and that the L1755 filament lies along it.

Figure 9*a* illustrates the wide range of percentage polarization observed in the Ophiuchus complex. The distribution has a mean of 3.6%, with a standard deviation of 2.2%, but the (somewhat ill-defined) peak of the distribution occurs at more like 4.3%, similar to the mean for the L1755 cloud alone. In Figure 9*b*, note the marked peak in the distribution of θ in Ophiuchus. The mean θ is 68°, with a standard deviation of 40°, but the peak of the distribution is again not centered on the mean, but is again closer to the value for L1755, at about 55°, as discussed in § IV*a* below.

Loren (1989*a*), in superposing the Vrba, Strom, and Strom (1976) Ophiuchus polarization measurements on his ^{13}CO maps, noted that the vector distribution was ordered on a large scale, but that for the L1689-L1712-L1729 filament (south of L1755 in Fig. 8), the peak in θ is $\gtrsim 20°$ from the elongation direction of the cloud. As is apparent in light of Figures 8, 9*b*, and Loren's (1989*a*) Figure 7, the majority of the polarization

[11] Measured as in L1506.
[12] Infrared polarimetry for ρ Oph cloud.

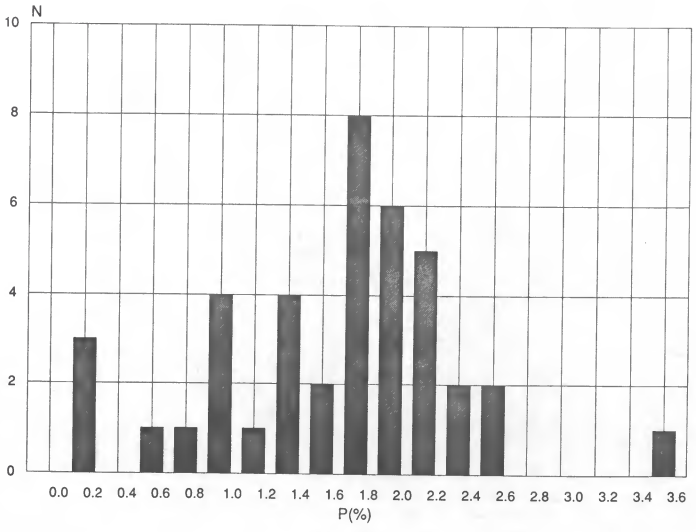

FIG. 2*a*

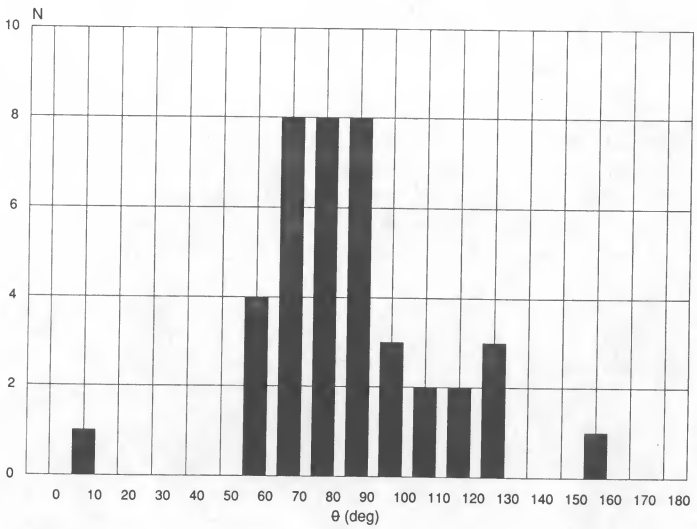

FIG. 2*b*

FIG. 2.—Distributions of (*a*) P (%) and (*b*) θ (degrees) for the L1506 polarization data illustrated in Fig. 1

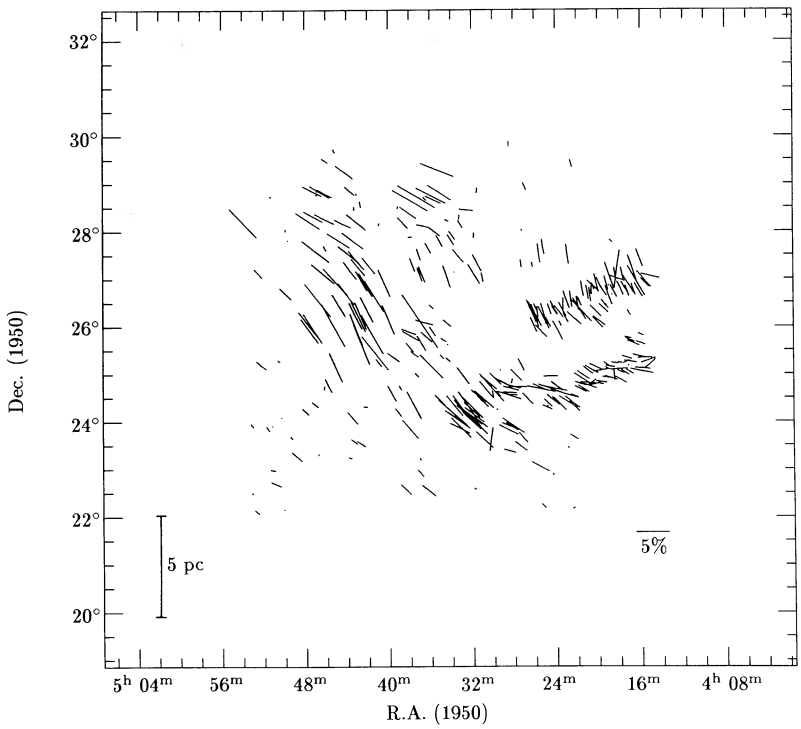

FIG. 3.—An optical polarization map of the region around the Taurus dark cloud complex. References are as follows: Heyer *et al.* (1987) [B216/217 region (near 04^h21^m; 26°30′) and B18 region (near 04^h27^m; 24°20′)]; this paper (L1506; see Fig. 1); Moneti *et al.* (1984) (all other observations shown).

vectors in Ophiuchus are rather well aligned with each other, and the individual clouds lie at various angles to the overall (large-scale average) polarization direction.

c) Perseus

The Perseus complex of molecular clouds is apparent on the optical photograph in Figure 10 as a series of connected regions of high extinction. From end to end, that is from L1448 to B5, the complex extends for about 40 pc, in projection, and the average projected "width" of the complex is about 5 pc.

The polarization data for the Perseus cloud are given in Table 3 and are plotted in Figures 11*a* and 11*b*. The polarization in the Perseus region seems to be of two different populations: one with a polarization of $\lesssim 1\%$ at an orientation of approximately 70°, and another one with ~ 1 to 3% polarization at an average position angle of 145°.

The distribution of P in Perseus, illustrated in Figure 12*a*, is not well characterized by its mean of 1.4% and a standard deviation of 1.4%. Instead, we note a peak at a value $\sim 0.7\%$, with a long falloff in the distribution toward higher polarizations. This trend reflects what is apparent in the polarization map (Figs 11*a*, 11*b*): there is a group of smaller (typically $\lesssim 1\%$) polarization vectors generally oriented at $\theta \approx 70°$, and another group of vectors for which P spans a large range, but is

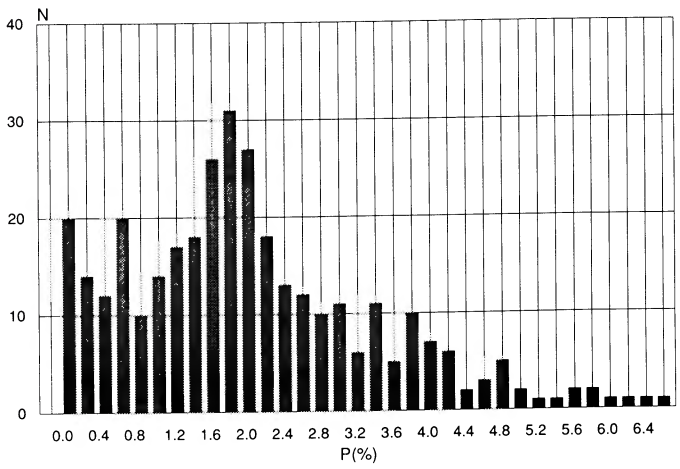

FIG. 4*a*

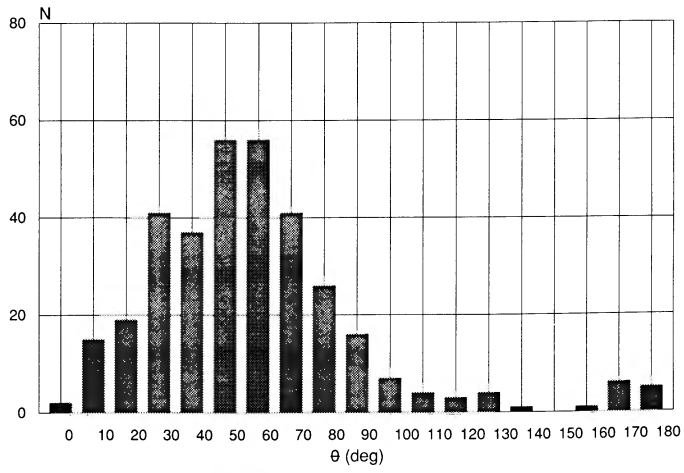

FIG. 4*b*

FIG. 4.—Distributions of (*a*) P (%) and (*b*) θ (degrees) for the Taurus polarization data illustrated in Fig. 3

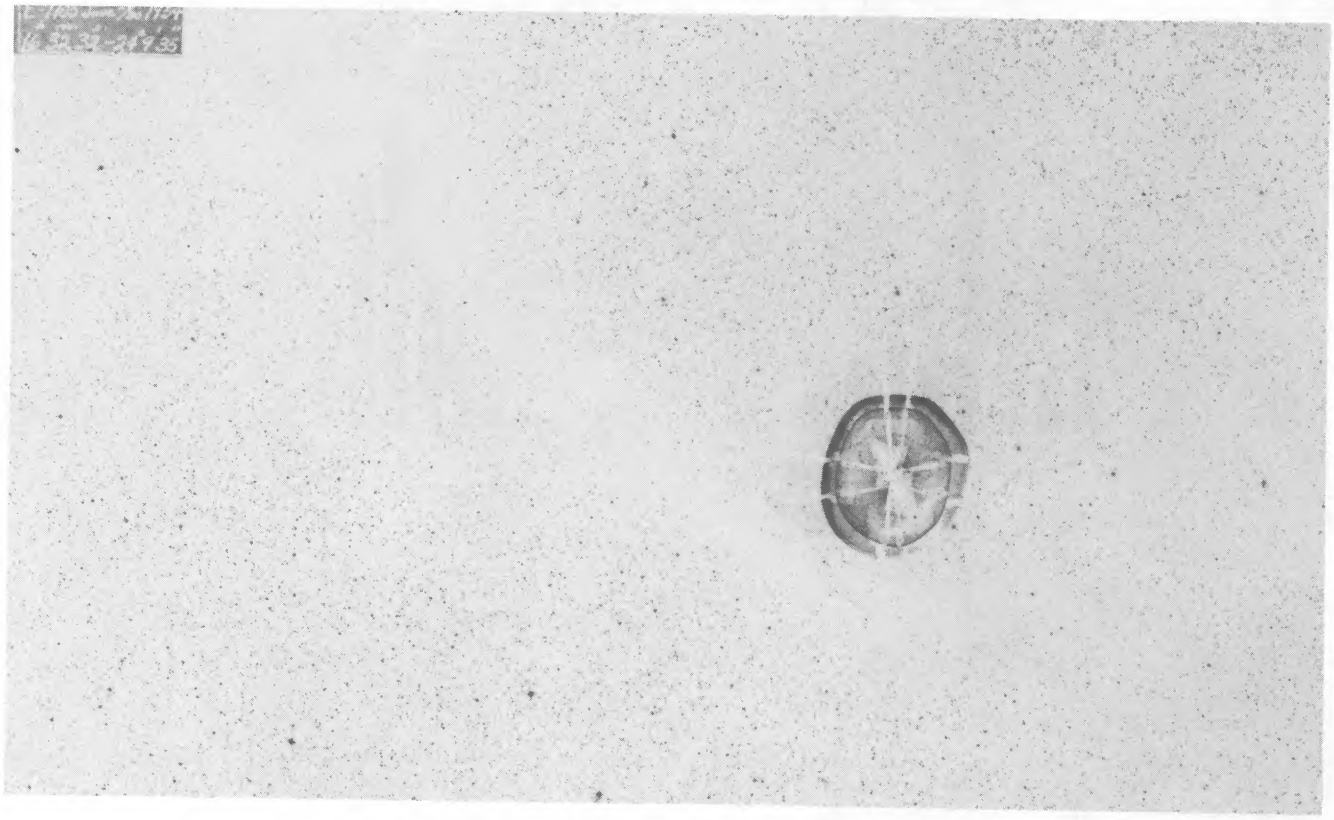

FIG. 5.—Optical photograph of the region around the L1755 dark cloud (reproduction of Palomar Sky Survey E-plate)

typically greater than 1%, oriented at about 145°. This bimodal distribution is strikingly apparent in Figure 12*b*, the distribution of θ for Perseus, which is discussed in further detail in § IV*b*. Neither the polarization map (Fig. 11*a*, 11*b*) nor the distribution of θ (Fig. 12*b*) is well characterized by the mean value of θ in Perseus.

The overall position angle of the Perseus cloud complex is difficult to define, since the clouds do not form a "filament" in projection, in the sense that L1506 and L1755 are filaments. Nonetheless, if we fit the bulk of the ^{13}CO emission shown in Figure 11*b* (Bachiller and Cernicharo 1986) by eye, we deduce a position angle of 65° E of N, which is similar to the $\sim 70°$ characterizing the distribution of $\lesssim 1\%$ polarization vectors.

The plane parallel to the galactic plane in this region, $b = -20°$, corresponds to 128° E of N near the center of the Perseus complex. This value is almost 20° away from the well-

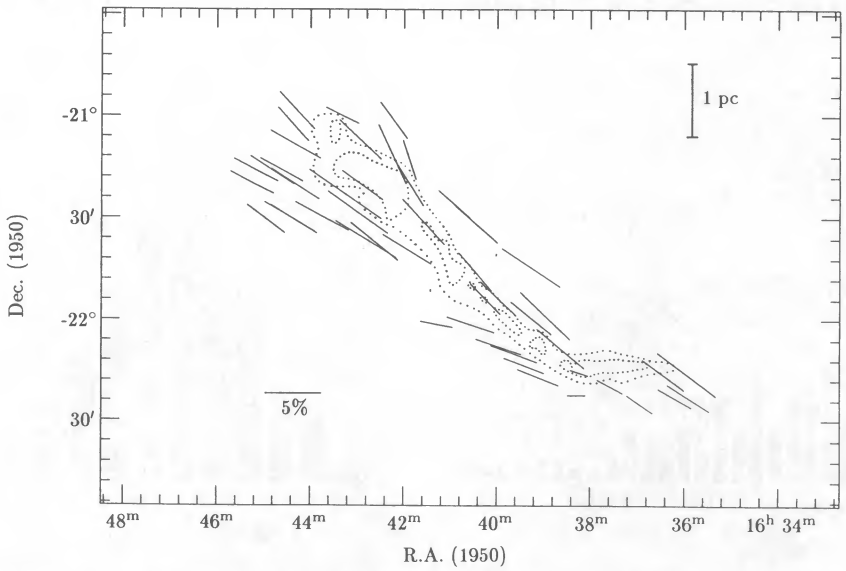

FIG. 6.—An optical polarization map of the region around the L1755 dark cloud, superposed on ^{13}CO ($J = 1$–0)T^*_R contours of 3 K and 5 K from Loren (1989*a*).

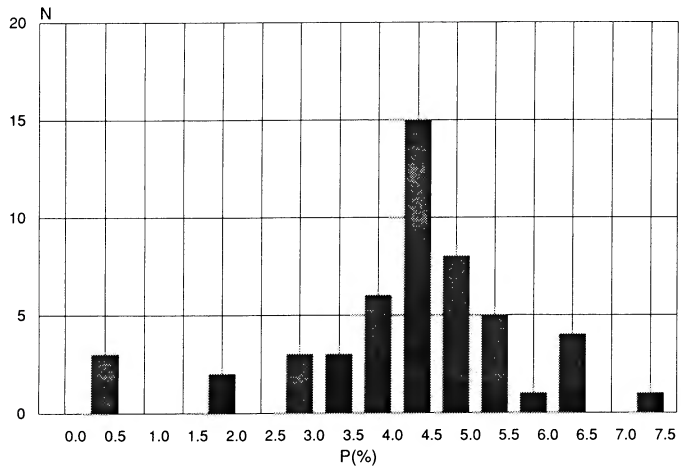

FIG. 7a

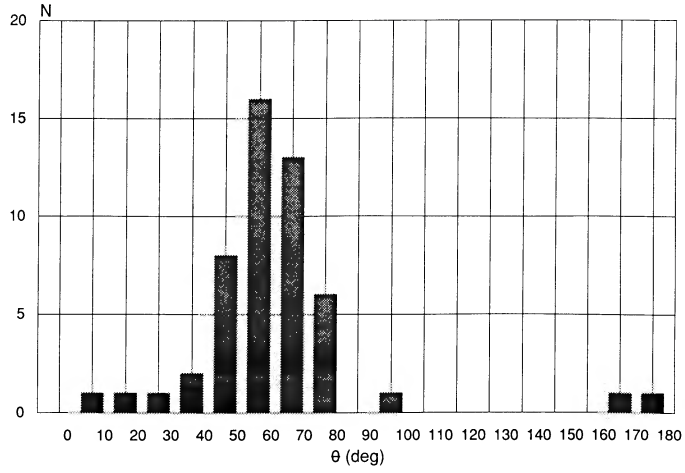

FIG. 7b

FIG. 7.—Distributions of (*a*) P(%) and (*b*) θ(degrees) for the L1755 polarisation data illustrated in Fig. 6

defined peak in θ at 145°, and it is of no immediately apparent significance.

IV. LARGE-SCALE DISTRIBUTIONS OF θ

Figures 3, 8, 11*a*, and 11*b* give us pictures of the projection, into the plane of the sky, of the magnetic fields which cross the lines of sight to the Taurus, Ophiuchus, and Perseus dark cloud complexes, respectively. In this section, we discuss possible three-dimensional field distributions which would give rise to polarization maps with the two-dimensional characteristics observed.

In attempts to de-project polarization maps of background starlight, we must realize that the "field direction" given by any particular polarization vector is actually the superposition of the polarizations produced at all points along the line of sight where aligned grains absorb photons from the (intrinsically unpolarized) background star. There can be several distributions of gas and dust, each with its own magnetic field direction, along the line of sight to a background star. These "gas and dust distributions" may be molecular clouds, or they may be less dense interstellar gas located between the observer and the background star. The field of primary interest, that associated with the cloud under study, may predominate, but we must appreciate that even this field is not necessarily perfectly uniform. It is more realistic to consider the field in a given cloud as having a straight, uniform, component, plus nonuniform perturbations.

The distributions of θ presented in Figures 4*b*, 9*b*, and 12*b* all exhibit clearly defined peaks, characterized by full widths ~30°. In addition, the distributions show a number of cases where θ seems randomly oriented. We model the distributions in terms of a "peak" direction ("uniform" field component), the dispersion about that peak (deviations from a perfectly

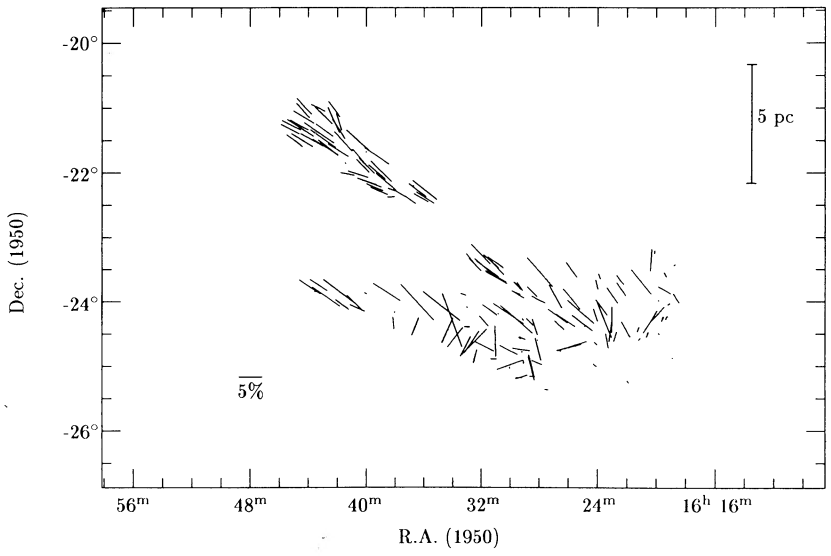

FIG. 8.—An optical polarization map of the Ophiuchus dark cloud complex. References are as follows: Vrba, Strom, and Strom (1976) [B42 region (all vectors south of −23°)]; this paper [L1755 region (all vectors north of −23°; see Fig. 6)].

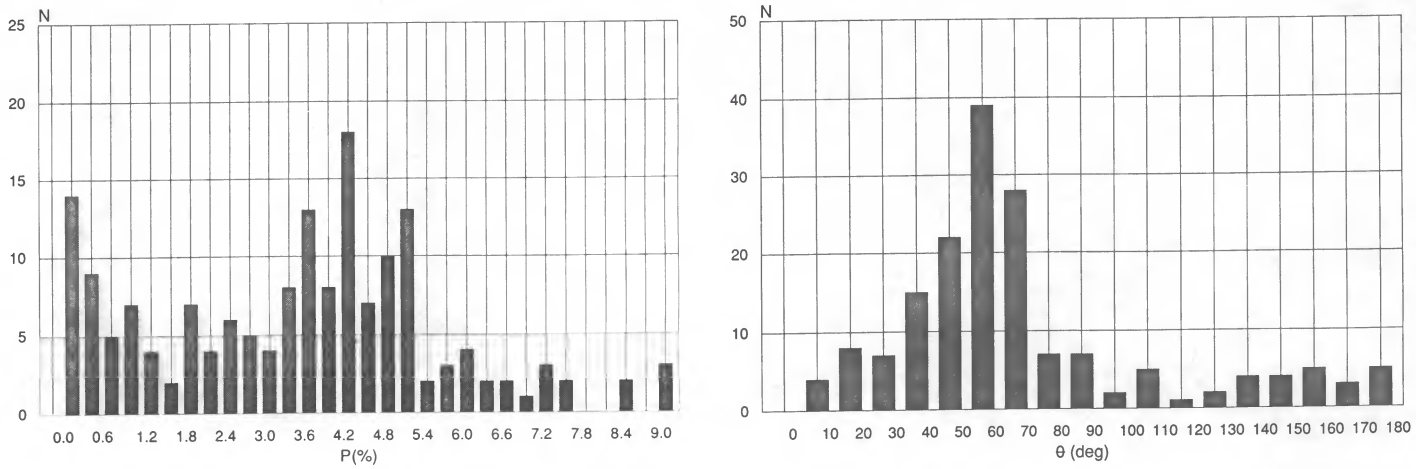

FIG. 9.—Distributions of (*a*) P (%) and (*b*) θ (degrees) for the Ophiuchus polarization data illustrated in Fig. 8

uniform field in the cloud of interest), and a "random" (baseline) component.

In most cases where a vector's θ is attributed to the "random" component of the distribution, the value of $P(\%)$ is small compared to the average value of $P(\%)$ for vectors whose θ is within one standard deviation of the peak θ. This difference can be explained if these "random" vectors coincide with minima in the extinction produced by the cloud of interest, where the less dense interstellar gas along the line of sight (associated with "random" fields) is primarily responsible for the observed polarization. In order to test this hypotheses carefully, one would need a large sample of polarization measure-

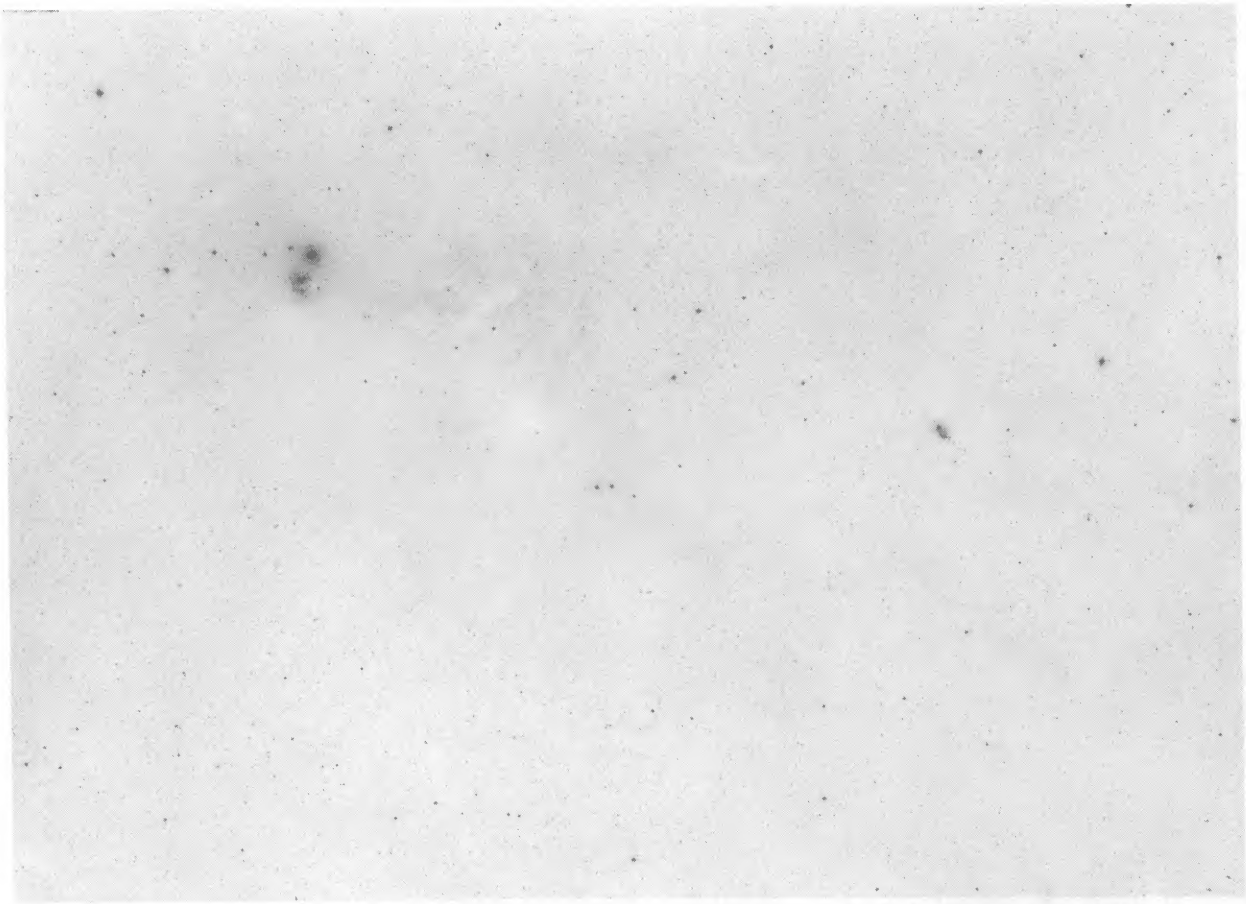

FIG. 10.—Optical photograph of the Perseus dark cloud complex (reproduction of Palomar Sky Survey E-Plate)

TABLE 3

PERSEUS POLARIMETRY

Star	R.A. (1950)	Decl. (1950)	P (%)	$\epsilon(P)$ (%)	θ (E of N)	$\epsilon(\theta)$	Star	R.A. (1950)	Decl. (1950)	P (%)	$\epsilon(P)$ (%)	θ (E of N)	$\epsilon(\theta)$
1.....	$3^h20^m31^s$	30°22′07″	1.15	0.10	80°	2°	46.....	3 32 48	30 52 54	1.19	0.10	60	2
2.....	3 20 48	30 24 33	0.78	0.09	82	3	47.....	3 32 48	31 24 03	1.46	0.10	146	2
3.....	3 21 15	30 05 28	0.02	0.06	145	6	48.....	3 32 49	30 52 52	1.21	0.10	59	2
4.....	3 22 17	29 53 15	0.13	0.10	106	21	49.....	3 33 02	31 08 53	0.11	0.10	132	26
5.....	3 22 42	30 34 01	0.64	0.09	76	4	50.....	3 33 30	30 54 36	0.34	0.08	110	7
6.....	3 22 45	30 45 23	1.38	0.09	110	2	51.....	3 33 33	30 53 26	4.48	0.21	146	1
7.....	3 23 24	29 58 34	1.14	0.07	85	2	52.....	3 33 35	31 21 20	1.12	0.06	156	2
8.....	3 23 25	30 36 50	1.97	0.09	121	1	53.....	3 33 37	31 24 46	1.67	0.11	69	2
9.....	3 24 13	29 51 49	0.55	0.09	76	5	54.....	3 34 20	31 30 15	0.44	0.11	62	7
10.....	3 24 25	30 32 51	1.33	0.05	119	1	55.....	3 34 27	30 48 59	4.69	0.10	145	1
11.....	3 24 28	30 45 02	0.06	0.09	5	43	56.....	3 34 39	30 57 07	5.06	0.10	152	1
12.....	3 24 35	31 28 21	2.41	0.09	96	1	57.....	3 35 18	31 02 13	9.14	0.13	150	1
13.....	3 24 47	31 38 55	2.00	0.09	101	1	58.....	3 35 26	31 27 55	1.90	0.13	136	2
14.....	3 25 02	31 00 17	1.21	0.08	49	2	59.....	3 35 29	31 47 05	1.23	0.09	137	2
15.....	3 25 11	29 50 59	0.65	0.09	78	4	60.....	3 35 47	31 14 19	0.62	0.09	75	4
16.....	3 25 29	30 35 26	0.85	0.09	70	3	61.....	3 35 52	31 14 22	4.27	0.17	133	1
17.....	3 25 42	30 12 13	0.97	0.02	177	1	62.....	3 36 09	31 18 43	0.10	0.18	147	52
18.....	3 25 47	29 46 57	1.78	0.10	1	2	63.....	3 36 12	31 38 32	1.05	0.10	139	3
19.....	3 26 27	30 00 23	0.85	0.11	125	4	64.....	3 36 24	31 53 51	0.46	0.10	77	6
20.....	3 26 36	31 18 59	0.60	0.14	51	7	65.....	3 36 38	31 26 54	0.40	0.10	78	7
21.....	3 26 54	31 19 17	0.75	0.10	49	4	66.....	3 37 08	31 53 08	0.40	0.11	74	8
22.....	3 27 04	30 12 31	0.88	0.09	73	3	67.....	3 37 09	32 00 02	0.12	0.10	119	23
23.....	3 27 09	31 23 12	0.15	0.17	101	32	68.....	3 38 15	31 45 16	1.95	0.09	163	1
24.....	3 27 21	30 36 42	0.56	0.10	67	5	69.....	3 39 04	31 59 09	2.33	0.10	145	1
25.....	3 27 31	30 20 11	1.02	0.09	93	3	70.....	3 39 53	32 00 08	2.31	0.09	148	1
26.....	3 27 34	31 26 47	0.09	0.09	48	31	71.....	3 40 03	31 17 16	2.00	0.23	6	3
27.....	3 28 06	31 28 06	1.37	0.10	20	2	72.....	3 40 17	32 08 39	2.74	0.09	154	1
28.....	3 28 24	30 20 46	0.76	0.10	87	4	73.....	3 40 19	31 20 46	3.10	0.11	50	1
29.....	3 28 38	30 30 50	0.87	0.08	69	3	74.....	3 41 16	32 20 30	0.79	0.16	27	6
30.....	3 28 48	30 45 43	1.14	0.09	17	2	75.....	3 42 01	32 25 29	2.28	0.10	140	1
31.....	3 28 60	31 30 48	2.93	0.11	144	1	76.....	3 42 05	31 18 11	3.14	0.10	54	1
32.....	3 29 02	30 19 29	0.24	0.10	27	12	77.....	3 42 15	32 29 41	3.18	0.10	79	1
33.....	3 29 06	31 19 41	0.49	0.11	63	6	78.....	3 42 20	32 08 20	0.63	0.06	39	3
34.....	3 29 38	30 20 12	0.21	0.09	114	13	79.....	3 42 49	32 03 49	0.40	0.09	53	7
35.....	3 29 58	30 24 23	0.51	0.09	87	5	80.....	3 43 02	32 38 00	0.58	0.09	43	5
36.....	3 30 04	30 40 12	0.43	0.09	143	6	81.....	3 43 13	31 55 34	1.48	0.10	155	2
37.....	3 30 20	31 16 51	4.34	0.10	154	1	82.....	3 43 17	31 36 41	2.34	0.11	34	1
38.....	3 30 45	30 28 18	2.29	0.10	141	1	83.....	3 43 25	31 29 04	0.59	0.09	145	5
39.....	3 30 49	31 00 00	1.24	0.10	72	2	84.....	3 43 51	31 41 09	0.88	0.09	27	3
40.....	3 31 10	30 51 24	1.10	0.10	70	3	85.....	3 43 53	32 25 46	1.31	0.10	3	2
41.....	3 31 34	30 57 55	0.42	0.11	80	8	86.....	3 44 02	32 44 48	2.06	0.10	142	1
42.....	3 32 16	30 38 06	3.58	0.11	125	1	87.....	3 45 13	32 40 32	0.53	0.10	62	5
43.....	3 32 23	31 03 43	0.02	0.12	161	52	88.....	3 46 01	32 40 13	0.59	0.10	57	5
44.....	3 32 34	30 45 49	0.66	0.10	74	4	Mean			1.40	0.10	92	8
45.....	3 32 46	31 05 08	0.34	0.11	70	9	Standard Deviation			1.42	0.03	45	23

NOTE.—The uncertainty in θ is given by the formula $\epsilon(\theta) = 28.^\circ65[\epsilon(P)/P]$ in cases where the uncertainty in P, $\epsilon(P) \ll P$, and $\epsilon(\theta) = 51.^\circ96$ otherwise (Serkowski 1974).

ments (along with accurate extinction values), including measurements of stars associated with very low as well as high extinction.

a) Taurus and Ophiuchus

In Figures 4*b* and 9*b*, clear, single peaks are visible in the distributions of θ. We model these peaks as single Gaussians[13] (which represent the well-ordered compont of the field in the cloud under study) superposed on a flat "baseline" (representative of random plane-of-the-sky fields along the line of sight). The baseline value in each case was taken to be the (nearest integer to the) mean of the bins outside of the apparent Gaussian component of the distribution.

[13] Gaussians are chosen simply as a representation of a function with well-understood deviations about the mean.

Table 4 summarizes the results we obtain using this technique and compares the fits with the means and standard deviations for the distributions (discussed in § III*a* and III*b*). The quantity $N_{\rm random}$ in Table 4 refers to the total number of cases attributed to the random (i.e., baseline) component in each cloud. In both Taurus and Ophiuchus, the total number of cases in the sample, N, is large (340 and 168, respectively) and relatively well distributed over the region (of the sky) of interest, so the results in Table 4 are a fair characterization of the large-scale field distributions.

In Taurus, we deduce that there is a "uniform" component of the field represented, for the distribution shown in Figure 4*b*, by a Gaussian centered at 48°, with a 1 σ dispersion of 23°. A baseline of three cases per 10° was subtracted before fitting. The number of cases included in this "random" component of the distribution amounts to 14% of the total, implying a large

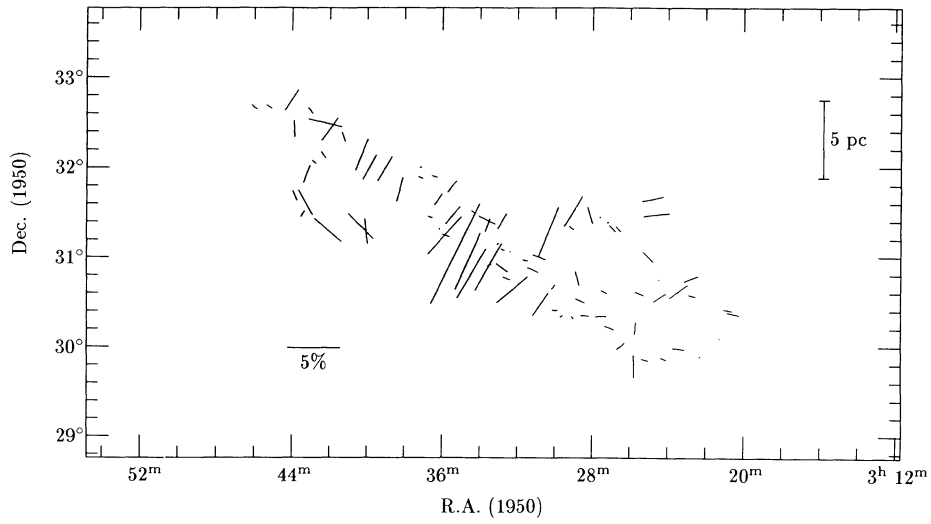

FIG. 11*a*

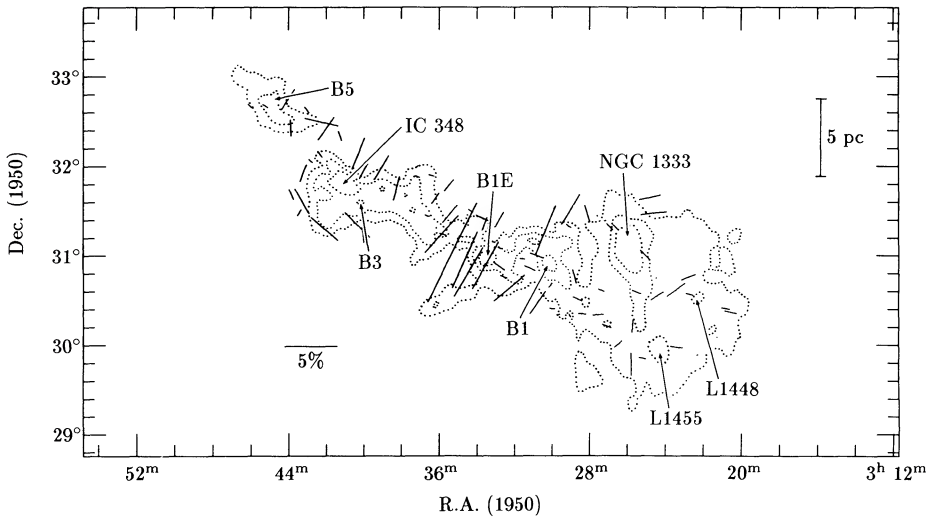

FIG. 11*b*

FIG. 11.—(*a*) An optical polarization map of the Perseus dark cloud complex. (*b*) Superposition of (*a*) on ^{13}CO ($J = 1$–0) integrated intensity contours of 2, 6, and 10 K km s^{-1} from Bachiller and Cernicharo (1986). Note: The length scale shown assumes a cloud distance of 350 pc.

(86%) fraction of the field is "ordered" (associated with the Gaussian component) in the plane of the sky.

In Ophiuchus, we use the sampe procedure to fit a Gaussian "uniform" component of the field at 55°, with a 1 σ dispersion of only 11°—a very sharp peak. The "random" baseline in this case consists of four cases per 10°, which amounts to 38% of the total number of cases. So, although the peak of the uniform component's distribution is sharper for Ophiuchus (Fig. 9*b*) than for Taurus (Fig. 4*b*), the random component of the distribution comprises more than double the percentage of the total number of measurements.

b) The Bimodal Distribution of θ in Perseus

The distribution of θ for the Perseus complex shown in Figure 12*b* is bimodal. So, after subtracting a baseline (corresponding to the "random" component of the distribution) of two cases per 10°, we separate the data into two groups, $\theta \leq 105°$ and $\theta > 105°$, before fitting *two* Gaussians, to represent the "uniform" components of the field. The results for each group are presented separately in Table 4 and compared with means and standard deviations for the separated data and with the overall mean and standard deviation.

The data are best fit by one Gaussian centered at 71° with a 1 σ dispersion of 12° and another Gaussian centered at 145°, with a 1 σ dispersion of just 8°. Together, these two Gaussians, representing the "uniform" fields in the clouds, make up about 60% of the data, and the remaining 40% is attributed to the random (baseline) component.

The 88 observations in Perseus (Table 3) are well distributed spatially in the complex, and their density is sufficient to show no sign of spatial distinction between the two distributions of θ observed. Apparently, these two very distinct plane-of-the-sky magnetic field components coexist in projection throughout the region of the Perseus complex from L1448 to B5.[14]

Turnshek, Turnshek, and Craine (1980, hereafter TTC) also notice a bimodal distribution of polarization vector position

[14] Principal condensations in Perseus are labeled in Fig. 11*b*.

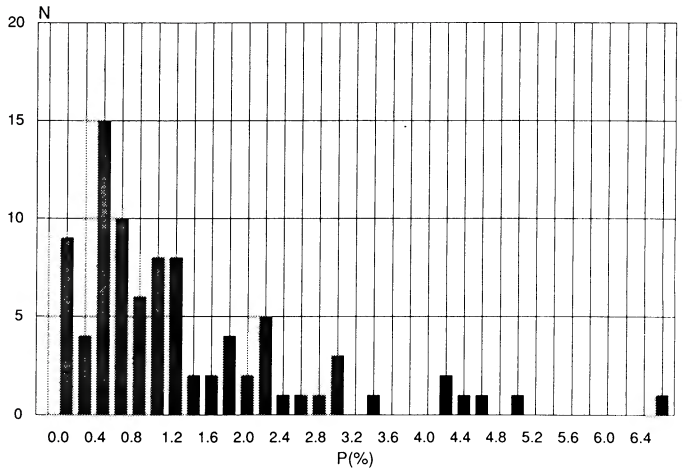

FIG. 12*a*

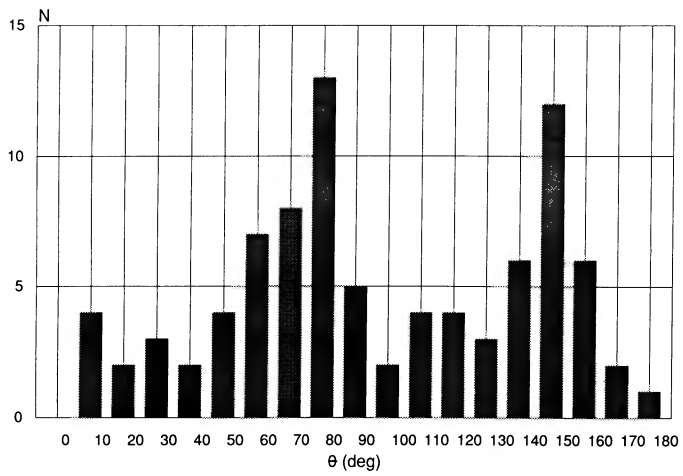

FIG. 12*b*

FIG. 12.—Distributions of (*a*) P (%) and (*b*) θ (degrees) for the Perseus polarization data illustrated in Figs. 11*a* and 11*b*

angles in a study of an extended region around NGC 1333, in Perseus. Their sample includes 22 stars, selected as very red from the Near Infrared Photographic Sky Survey (NIPSS; Craine *et al.* 1979). For this region, they observe peaks in the distribution of position angle at 87° ± 24° and 147° ± 9°, consistent within one standard deviation with the fitted peaks listed in Table 4.

TTC proposed that the observed bimodal distribution of θ is due to a two-cloud structure in the NGC 1333 region, so that the observed linear polarization is the result of two separate dust distributions along the line of sight, each associated with a different field orientation. They support their hypothesis by noting Loren's (1976) observations which revealed two velocity components ($v_{LSR} \approx 6.3$ and 8.3 km s^{-1}) in the dense gas surrounding NGC 1333. TTC further suggest that there is a spatial correlation where polarizations associated with one peak in θ come from one region in relation to NGC 1333, and the others from another.

Vrba, Strom, and Strom (1976) have measured polarizations in the region immediately surrounding NGC 1333, more on the size scale of Loren's (1976) maps, and although it is not immediately obvious upon inspection of their map, they too find a bimodal distribution of θ (peaked at 15° ± 15° and 105° ± 15°). They conclude that the distribution "suggests the possibility of two clouds superposed along the line of sight, each having a rather uniform distribution of polarization position angles."

In the B5 region, at the eastern end of the Perseus complex, Joshi *et al.* (1985) measured the polarization of 20 stars. Using their data, one can plot the distribution of polarization vector angles and note that it also has two peaks, one at a mean of 45°, with a standard deviation of 24°, and the other at a mean of 144°, with a standard deviation of 16°. Although the sample is small, these peaks are remarkably similar to both the TTC result, and to the peaks found in the distribution of θ shown in Figure 12*b* and listed in Table 4. In addition, the polarizations (P) of the stars included in the B5 144° peak are all $\geq 1.5\%$, consistent with the pattern observed throughout Perseus of this orientation being generally correlated with larger polarizations.

The bimodal distribution of θ observed in Perseus can be explained by a change in the plane-of-the-sky magnetic field orientation along the line of sight. The two distinct field orientations observed may correspond to (at least) two-cloud complexes located at different distances along the line of sight. Loren (1976), TTC, and Vrba, Strom, and Strom (1976) all favor a two-cloud hypothesis for the NGC 1333 region, and our data indicate that such a two-cloud trend may extend throughout the Perseus complex. The spatial correlation in θ deduced by TTC may be an artifact produced by sampling a spatially limited piece of a larger distribution.

In a large-scale (30′ resolution) ^{12}CO map of the Taurus-Perseus-Auriga region, Ungerechts and Thaddeus (1987) identified an extensive projected area in the region of Perseus from

TABLE 4

SUMMARY OF STATISTICS ON LARGE-SCALE POLARIZATION MAPS

SAMPLE	N	MEAN θ (E of N)	STANDARD DEVIATION	GAUSSIAN FIT: Peak θ (E of N)	GAUSSIAN FIT: σ	BASELINE $\frac{N_{random}}{N} \times 100$ (%)
Taurus, all data	340	54	33	48	23	14
Ophiuchus, all data ...	168	68	40	55	11	38
Perseus, all data	88	92	45	N/A	N/A	40
Perseus, $\theta \leq 105°$	54	60	25	71	12	41
Perseus, $\theta > 105°$	34	141	15	145	8	38

IC 348 to NGC 1333, where the spectra consist of two velocity components, which appear partly blended or fully separated. As one of a number of possible explanations, they suggest that the velocity structure is attributable to two layers of clumpy clouds well separated (by 100–200 pc) along the line of sight, but very close in velocity (< 2 km s^{-1}).

This complicated velocity structure in Perseus is observed in other molecular transitions, at finer resolutions, as well. Using OH 1665 and 1667 MHz observations with 15′ resolution, Goodman *et al.* (1990) find that certain clumps in Perseus have a systematic velocity different from that of neighboring clumps by more than one FWHM line width. And in ^{13}CO maps, made with $\sim 1'$ resolution (Bally 1989), fine-scale wispy structures can be seen to extend from clumps, but not to connect clumps in velocity space to their neighbors.

These velocity patterns are quite different from the small ($\lesssim 1$ FWHM) line width), often systematic, velocity gradients observed in Taurus (Ungerechts and Thaddeus 1987, Fig. 6*c*) and Ophiuchus (Loren 1989*b*, Fig. 2*a*). Hence, the Perseus molecular cloud "complex" may well be a superposition of distinct cloud structures, with significant separations along the line of sight.

If the bimodal distribution of θ in Perseus arises from at least two "complexes" of molecular clouds, superposed along the line of sight, then the extinction ($\propto$ column density) in the nearer cloud(s) must be low ($A_V \lesssim 1$ mag), and/or it must have significant fluctuations, in order to see "through" to the farther cloud.

There are also other plausible scenarios which could give rise to the observed bimodal distribution of θ in Perseus. An extended H I/dust "atomic" cloud (not associated with star formation), pervaded by an ordered field, between us and the "molecular" clouds in Perseus could be responsible for one component of the observed polarization. Or, the observed pattern could be produced by a change in the plane-of-the-sky field direction within a single molecular cloud, rather than a change in the plane-of-the-sky field in the space between two separate clouds which appear superposed along the line of sight. Considering the molecular line evidence for two distinct velocity distributions discussed above, however, we favor the hypothesis that there are (at least) two "patchy" molecular clouds along our line of sight to Perseus.

V. DISCUSSION

a) Polarization Observations

The average polarization-to-extinction ratio, P/A_V (Table 5), is of order 2% mag^{-1} in Taurus, Ophiuchus, and Perseus, a value consistent with the polarization observed having been produced by aligned dust grains (Davis and Greenstein 1951). At galactic latitudes of $b \approx -17$, 15, and $-20°$, Taurus, Ophiuchus, and Perseus are all substantially out of the galactic plane, as well as being at distances ≤ 350 pc. Hence we can safely assume that most of the extinction and polarization observed is not due to general galactic interstellar dust (which would give extinctions < 0.4 mag), but is instead produced predominantly by dust associated with the molecular clouds of interest.

It is thus likely that the polarizations presented in this paper are caused by selective extinction due to magnetically aligned grains in the clouds of interest. However, it is important to take into account the following cautions in analyzing polarization maps:

1. The field we observe is only the plane-of-the-sky component of what could actually be a far more complicated field in three dimensions.

2. The efficiency with which grains produce polarization may be reduced in dense molecular clouds, despite a potentially stronger magnetic field, in comparison with lower density regions. Many grain alignment schemes depend on grains being continuously stabilized by "suprathermal" (Purcell 1979) rotation, produced mainly by the recoil of the hydrogen molecule in the reaction $H + H \rightarrow H_2 + 4.5$ eV, which occurs preferentially at active sites (Hollenbach and Salpeter 1971) on the surface of grains. Therefore, the grain alignment process can become less efficient where the H I density is sufficiently low, as in the densest regions of molecular clouds, where a relatively small fraction of the hydrogen is atomic (see Johnson 1982). So, polarization maps of "molecular" clouds may only illustrate the plane-of-the-sky magnetic field which threads regions where the abundance of H and grains is enough to produce alignment. This field may or may not continue through to the smaller, denser, more "molecular" clouds. Furthermore, detailed studies (Clayton and Cardelli 1988) conclude that large grains (thought to be associated with the denser regions of the cloud; Carrasco, Strom, and Strom 1973) are not efficient at producing polarization, either because a smaller axial ratio lowers the ability of the grain to polarize light, or because a reduced alignment efficiency (in regions where grains are large) means that fewer grains are aligned.

3. Many grain alignment theories predict alignment time scales $\sim 10^6$ yr,[15] which are only a factor of 10 less than cloud

[15] Dragovan (1986) presents sample time scales, based on the theories of Davis and Greenstein (1951, paramagnetic relaxation); Dolginov and Mytrophanov (1976, the Barnett effect which leads to suprathermal rotation) and Purcell 1979, a combination of suprathermal rotation with paramagnetic relaxation and the Barnett effect).

TABLE 5

SUMMARY OF QUANTITIES RELATED TO $\boldsymbol{B}$

Cloud Complex	Mean P (%)	A_V[a] (mag)	Reference	P/A_V (% mag^{-1})	$B_\parallel$[b] (μG)	Reference	B_{eq}[c] (μG)	Reference	$B_\parallel/B_{eq}$[d]
Taurus	2.1	1.0	1	2.1	<10–15	2, 3	32	2, 4	0.4
Ophiuchus	3.6	1.6	1	2.2	10	5	26	6	0.4
Perseus	1.4	0.8	7	1.8	12–27	3, 4	25	2, 4	0.8

[a] Corresponding to local ^{13}CO $J = 1$–0 detectability threshold.

[b] OH Zeeman observations, relevant to scales ~ 0.1 to ~ 1 pc, all made at either NAIC Arecibo 305 m (refs [3] and [4]) or NRAO Green Bank 43 m (refs [2] and [5]).

[c] Derived, as described in § V*b*, from OH data in regions where OH Zeeman observations have been made.

[d] Calculated by taking a representative (average) value of $B_\parallel$.

REFERENCES.—(1) Frerking, Langer, and Wilson 1982; (2) Crutcher *et al.* 1990; (3) Goodman *et al.* 1989; (4) Goodman *et al.* 1990; (5) Crutcher 1988; (6) Myers *et al.* 1978; (7) Bachiller and Cernicharo 1986.

lifetimes ($\sim 10^7$ yr), assuming field strengths of no more than tens of μG, as measured in Zeeman experiments. Therefore, an excess of de-aligning collisions, produced by shocks and/or other kinetic phenomena (e.g., outflows, supernovae), which have shorter time scales, may not permit the (slow) magnetic alignment of grains in certain regions.

Furthermore, we note that the polarization of background starlight observed is produced only by dust grains which are coincident, in projection, with the stellar disk. If a background star with the radius of the Sun is located at 4 times the distance to the cloud of interest, the angle subtended by the star at the cloud corresponds to a linear size of about 10^{-8} pc. In this sense, polarization maps of the sort presented here are highly undersampled: the distance between measurements (typically arcminutes) far exceeds the size of the "beam" (typically $\sim$micro-arcsec), which is determined by the projected stellar diameter. The "ordered" appearance of maps of polarization of background starlight does imply that there is a large-scale field spanning the large number of missing beams, but we must realize that we are not sensitive to perturbations smaller than the projected distance between stars observed ($\sim$0.05–1 pc) for the maps presented here), and that each polarization vector observed is produced by all (not necessarily similarly) aligned grains within the volume cut through the cloud by an individual star's light.

b) *The Magnetic Field in Three Dimensions*

Observations of the polarization of background starlight give information about a two-dimensional (plane-of-the sky) projection of a three-dimensional magnetic field. In § IV, we modeled this projection as a "uniform" field direction, with "nonuniform" perturbations about that direction, and a "random" component. Since the observational accuracy in measuring θ is typically better than 3°, and the 1 σ dispersion of the Gaussian fits to the distributions of θ is typically at least 10°, we can conclude either that there is a statistically significant "non-uniform" component to the magnetic field in molecular clouds, or, alternatively, that grains have not had time to align in all parts of the clouds. For the sake of argument, we hypothesize below that the grain alignment time ($\sim 10^6$ yr; see Purcell 1979; Dragovan 1986; Goodman 1989) in gas with $A_V \sim 1$ mag is a small enough fraction of the cloud lifetime ($\sim 10^7$ yr; e.g., Kwan 1988) so that the latter possibility can be dismissed.

Some of the dispersion in the distributions of θ is due to large-scale bending of the field lines over the tens of pc spanned by the largest maps. In Taurus, the largest map we present (Fig. 3), the mean field direction changes by as much as 52° from one part of the map to another, comparable to the FWHM of the distribution of θ (Fig. 4*b*). But if we look more closely, on a finer scale, we seen that even in individual filamentary clouds such as L1506 (Fig. 1) and L1755 (Fig. 6), where the mean field direction is constant, in that it does not smoothly bend across the cloud as in the Taurus map, there is still a large "non-uniform" component of the field, as evidenced by the 20°–30° widths in the distributions of θ for these clouds (see Figs. 2*b* and 7*b*).

There are at least two subtly distinct ways to physically model the "nonuniform" component in the distributions of θ: (1) as smooth fluctuations in the field (waves), or (2) as tangling in the field (random three-dimensional fluctuations in $\boldsymbol{B}$). Soon after the polarization of background starlight had been discovered (Hiltner 1949; Hall 1949), Chandrasekhar and Fermi (1953) proposed that the undulations in the patterns formed by the polarization vectors were due to hydromagnetic waves. Under this hypothesis, they used the dispersion in θ for polarizations measured in the plane of the galaxy to successfully estimate the "background" magnetic field in the spiral arms to be about 3 μG, a number since confirmed by numerous observations (see Troland and Heiles 1986). The dispersions in θ we observe could similarly be attributed to hydromagnetic waves. Or, alternatively, instead of modeling the deviations from a straight field as waves, we could consider the "non-uniform" component of the field to be the projection of a set of random three-dimensional fluctuations. In this picture, the field we observe, $\boldsymbol{B}_\perp$, could then be considered as the superposition of a straight field and a randomly oriented (tangled) field.

In addition to decomposing $\boldsymbol{B}_\perp$ into its constituent "uniform" and "nonuniform" components, we can also ask what fraction of B, the total magnetic field strength, is represented by $|\boldsymbol{B}_\perp|$.

Table 5 presents values of $B_\parallel$, the line-of-sight field strength for regions of OH emission ($n \gtrsim 10^3$ cm^{-3}; $A_V \sim 6$ mag) in Taurus, Ophiuchus, and Perseus. (Note that these OH condensations are typically associated with individual star-forming "cores" within a dark cloud complex.) Although we cannot directly reconstruct the three-dimensional field ($\boldsymbol{B}$) by combining our polarization measurements with the (Table 5) Zeeman measurements, we *can* use the information we do have about the perpendicular and parallel field components to draw general conclusions about the field.

For example, if we hypothesize that the percentage of polarization we observe (per magnitude of extinction) in clouds whose properties are otherwise similar (i.e., similar temperature, similar grains) increases monotonically with $B_\perp$, then the mean value of P/A_V in a cloud gives us an indication of how large a component of $\boldsymbol{B}$ is represented by $\boldsymbol{B}_\perp$. Under this hypothesis, the mean values of P/A_V listed in Table 5 marginally indicate that Perseus has less of a component of its $\boldsymbol{B}$ in the plane of the sky than does Taurus or Ophiuchus.

Clouds with similar properties (density, line width [Δv], size [R]), also have similar "equilibrium" fields, B_{eq}. We define B_{eq} as the field for which the cloud's magnetic energy equals its kinetic energy. For clouds where the thermal kinetic energy is negligible, $B_{eq} = 15\Delta v^2/R$ (Myers and Goodman 1988*a*, *b*). As is apparent in Table 5, the values of B_{eq} for the regions where the Zeeman observations have been made are all extremely similar, $\sim$30 μG. Therefore, *if* the total field has a constant relationship with the equilibrium field from cloud to cloud, the ratio $B_\parallel/B_{eq}$ gives an indication of the inclination angle of $\boldsymbol{B}$ to the line of sight. Based on the values of $B_\parallel/B_{eq}$ in Table 5, we would again deduce that the field in Perseus is oriented more along the line of sight than is the field in Taurus and Ophiuchus.

As a final comment on the magnetic field in Perseus, we note that the mean value of $P(\%)$ for the $\theta \leq 105°$ "cloud" is less than 1%, making it more than a factor of 2 smaller than the mean values of $P(\%)$ in Taurus, Ophiuchus, and the $\theta > 105°$ "cloud" in Perseus. The low measured values of $P(\%)$ could be caused by very low extinction in the polarizing dust cloud, or, by the arguments given above, they could imply that the field in the cloud characterized by whatever v_{LSR} corresponds to these vectors is mostly along the line of sight. The latter explanation would be verified if the Zeeman effect were more easily detected (with $B_\parallel \sim B_{eq}$) in OH condensations in Perseus associated with the v_{LSR} corresponding to the $\theta \leq 105°$ dis-

tribution of polarization vectors. At present, all the Zeeman effect observations in Perseus are clustered near B1, at ~ 6 km s^{-1} (Crutcher *et al.* 1990; Goodman *et al.* 1989, 1990), but future observations may shed light on this question.

c) *The Role of the Magnetic Field*

The magnetic field direction traced by polarization observations shows little variation over $\gtrsim 10$ pc size scales, while individual clouds within a complex are oriented at a wider variety of angles to the overall field pattern. Indeed, the orientation of some clouds, such as L1755 ($\sim 0°$ to the mean θ) and B216–B217 ($\sim 90°$ to the mean θ; Heyer *et al.* 1987), does cause them to appear "parallel" or "perpendicular" to the pattern of polarization vectors observed. Yet, still, when even L1755 and B216–B217 are placed in the context of the larger scale cloud and field distribution, we see that these individual clouds' projected special orientation to the large-scale field is likely partly due to a magnetic field, and partly due to chance.

Considering the orientations observed, we can ask the following questtons about the cloud/field interaction at the size scales traced by the polarization maps we have presented.

Does the magnetic field "control" cloud structure?—If this were true, in an absolute sense, we would expect to see more "alignment" between cloud features (e.g., elongation, rotation, molecular outflows), and the magnetic field than is immediately apparent. In his study of the Ophiuchus cloud complex, Loren (1989*a*) concludes that most of the cloud structure is due to shock encounters and that the irregularities in the field are the result of shocks as well. Heyer (1988), in a study of ^{13}CO emission in the Taurus molecular cloud, finds that the projected orientations of dense cores within dark clouds and projected rotational axes are not systematically aligned with the local plane-of-the-sky field direction, as given by polarization maps. Heyer's (1988) sample is relatively small, yet there is no systematic study to date which illustrates that core and cloud axes, and their respective rotational axes *are* aligned in an entirely systematic way with the plane-of-the-sky field. In L1641, Strom *et al.* (1986) find that the projected axes of five out of six young stellar outflows, separated by ~ 10 pc are oriented within 30° of the magnetic field. And, Cohen, Rowland, and Blair (1984) report alignment of five out of 10 outflows (located in assorted regions on the sky) within $\pm 20°$ of their local $B_\perp$, as traced by optical polarization measurements. The energetic significance of these "alignments" will be more clear after more examples are included in the sample, and after careful statistical consideration of the projection of three-dimensional relative orientations into two dimensions. The evidence to date, though, shows that the magnetic field does not have an "iron" grip on dark clouds, and the interesting problem is to quantify the energetics and physics of the grip it does have.

Does cloud structure "control" the magnetic field?—In many polarization maps, it appears that the field is unaffected by the presence of density enhancements. Not only, as discussed above, is the magnitude of the polarization relatively unchanged; in addition, the plane-of-the-sky orientation of the field, as given by the polarization of background stars where the line of sight passes through dark clouds, is very close to the overall field orientation in the plane of the sky surrounding them. In Taurus (see Fig. 3 and Moneti *et al.* 1984), there are no obvious kinks or even wiggles in the pattern of polarization vectors which could be associated with the presence of dark clouds. In L204 (McCutcheon *et al.* 1986), a similar situation exists. The pattern of polarization in the dark cloud L204 is basically E-W, which, as pointed out by Heiles (1988), is close to the average large-scale (~ 100 pc) plane-of-the-sky field direction in the region. In addition, the L204 filament is not a simple N-S filament, but instead it is actually S-shaped, and the polarization vectors do not follow the overall "perpendicular to the cloud axis" pattern on the smaller (~ 1 pc) scale. Therefore, it is possible that the field revealed by polarization observations in the L204 dark cloud, and in the Taurus dark clouds, is basically an ambient field, and that the presence and orientation of the dense condensations have little to do with the ambient field geometry.

VI. SUMMARY AND CONCLUSIONS

In polarization maps of individual highly elongated dark clouds (L1506 and L1755), we find there to be a well-defined peak magnetic field direction in the plane of the sky, as others have previously found in studies of similar clouds. We also find that there is always a finite dispersion about that peak, which is much larger than the instrumental uncertainty in the measurement of θ, but smaller than would be expected for a random distribution of field distributions. Large-scale polarization maps (of Taurus, Ophiuchus, and Perseus) show similar scatter about their mean field directions. We attribute the dispersion about the peak θ to nonuniform perturbations in the field, either wavelike or random.

In the large-scale polarization maps of the Taurus and Ophiuchus molecular cloud complexes, it is evident that the dispersion in the position angle of filamentary clouds within the complex generally exceeds the dispersion in the position angle of the magnetic field, as traced by the polarization vectors. For individual dark clouds, this implies that clouds which appear elongated on the plane of the sky are *not all associated with a pattern of polarization vectors particularly "parallel" or "perpendicular"* to their geometry. Instead, clouds tend to be oriented at the angle formed by their long axis and the "mean" direction of the local *large-scale* field. Thus, L1755 appears "perfectly" aligned with its local magnetic field direction, yet L1506 appears to deviate by a significant amount (23°) from its local field, while the field in each cloud fits in smoothly with the surrounding large-scale field geometry.

In the large-scale polarization map of the dark cloud complex which extends from L1448 to B5 in Perseus, we find a bimodal distribution of θ, which has also been found in previous, smaller, polarization maps of clouds in this region. We explain the distribution of θ as resulting from at least two distributions of gas along the line of sight (each with their own local $\boldsymbol{B}_\perp$) which appear as a "complex" in projection. This hypothesis is supported by molecular spectral line observations which show gas in two distinct ranges of v_{LSR} along the line of sight.

The data in this paper suggest many observational and theoretical problems which should be addressed in the near future. Most apparent is the need to study the origin of the bimodal distribution of θ in Perseus, by assigning velocities (and distances) to clouds, and measuring extinctions and distances to the background stars. More polarization measurements of stars background to the "empty" portions of a molecular cloud complex (i.e., *not* associated with high extinction), and polarization measurements in clouds at high galactic latitude, isolated from the magnetic field and dust of the galactic plane

(see Seki 1990), will point out the similarities and/or differences between polarization produced by grains associated with lines of sight coincident with dark clouds, and polarization produced by the large-scale interstellar medium.

Future study of potentially aligned features in molecular clouds, e.g., projected cloud elongation, rotation, outflow axes, *and* the polarization of background starlight, will help us to understand the relationships between the many physical processes contributing to the phenomena observed, including the magnetic field's role in the observed alignments or non-alignments. The degree of "alignment" will need to be carefully quantified using a statistical analysis which includes the properties of the projection of three-dimensional relative orientations into two dimensions, and vice versa.

We would like to thank L. Greenhill for his versatile plotting software and helpful comments on the manuscript. We are grateful to M. Jamil for her tireless data entry. We also thank R. McMillan and P. Houlahan for providing unpublished, precessed coordinates for the Moneti *et al.* (1984) data. We thank T. Troland (the referee) for his sage comments. A. A. G. Thanks Zonta International for an Amelia Earhart Fellowship. P. B and F. M. are grateful to the Natural Sciences and Engineering Research Council (NSERC) of Canada for financial assistance.

REFERENCES

Angel, J. R. P., and Landstreet, J. D. 1970, *Ap. J. (Letters)*, **160**, L147.
Bachiller, R., and Cernicharo, J. 1986, *Astr. Ap.*, **166**, 283.
Bally, J. 1989, private communication.
Bastien, P. 1982*a*, *Astr. Ap. Suppl.*, **48**, 153.
———. 1982*b*, *Astr. Ap. Suppl.*, **48**, 513.
Bastien, P., Drissen, L., Ménard, F., Moffat, A. F. J., Robert, C., and St.-Louis, N. 1988, *A.J.*, **95**, 900.
Bertiau, F. C. 1958, *Ap. J.*, **128**, 533.
Carrasco, L., Strom, S. E., and Strom, K. M. 1973, *Ap. J.*, **182**, 95.
Chandrasekhar, S., and Fermi, E. 1953, *Ap. J.*, **118**, 113.
Clayton, G. C., and Cardelli, J. A. 1988, *A.J.*, **96**, 695.
Cohen, R. J., Rowland, P. R., and Blair, M. M. 1984, *M.N.R.A.S.*, **210**, 425.
Craine, E. R., Duerr, R. E., Horner, V. M., Imhoff, C. L., Routsis, D. E., Swihart, D. L., and Turnshek, D. A. 1979, *NIPSS Contribution*, Ser. A., No. 3 (Tucson: Steward Observatory).
Crutcher, R. M. 1988, in *Lecture Notes in Physics*, Vol. **315**, *Molecular Clouds in the Milky Way and External Galaxies*, ed. R. L. Dickman, R. L. Snell, and J. S. Young (Berlin: Springer), p. 105.
Crutcher, R. M., Goodman, A. A., Heiles, C., Kazés, I., Myers, P. C., and Troland, T. H. 1990, in preparation.
Davis, L., and Greenstein, J. L. 1951, *Ap. J.*, **114**, 206.
Dolginov, A. Z. 1990, in *IAU Symposium 140, Galactic and Extragalactic Magnetic Fields*, ed. R. Beck, P. P. Kronberg, and R. Wielebinski (Dordrecht: Kluwer), in press.
Dolginov, A. Z., and Mytrophanov, I. G. 1976, *Ap. Space Sci.*, **43**, 291.
Dragovan, M. 1986, *Ap. J.*, **308**, 270.
Elias, J. H. 1978, *Ap. J.*, **224**, 857.
Frerking, M. A., Langer, W. D., and Wilson, R. W. 1982, *Ap. J.*, **262**, 590.
Goodman, A. A. 1989, Ph.D. thesis, Harvard University.
Goodman, A. A., Crutcher, R. C., Heiles, C., Kazés, I., Myers, P. C., and Troland, T. H. 1990, in preparation.
Goodman, A. A., Crutcher, R. C., Heiles, C., Myers, P. C., and Troland, T. H. 1989, *Ap. J. (Letters)*, **338**, L61.
Hall, J. S. 1949, *Science*, **109**, 166.
Heiles, C. 1988, *Ap. J.*, **324**, 321.
Herbig, G. H., and Jones, B. F. 1983, *A.J.*, **88**, 1040.
Heyer, M. H. 1988, *Ap. J.*, **324**, 311.
Heyer, M. H., Vrba, F. J., Snell, R. L., Schloerb, F. P., Strom, S. E., Goldsmith, P. F., and Strom, K. M. 1987, *Ap. J.*, **321**, 855.
Hiltner, W. A. 1949, *Science*, **109**, 165.
Hollenbach, D., and Salpeter, E. E. 1971, *Ap. J.*, **163**, 155.
Johnson, P. E. 1982, *Nature*, **295**, 371.
Joshi, U. C., Kulkarni, P. V., Bhatt, H. C., Kulshrestha, A. K., and Deshpande, M. R. 1985, *M.N.R.A.S.*, **215**, 275.
Kwan, J. 1988, in *Molecular Clouds in the Milky Way and External Galaxies*, ed. R. L. Dickman, R. L. Snell, and J. S. Young (Berlin: Springer), p. 281.
Loren, R. B. 1976, *Ap. J.*, **209**, 466.
———. 1989*a*, *Ap. J.*, **338**, 902.
———. 1989*b*, *Ap. J.*, **338**, 925.
McCutcheon, W. H., Vrba, F. J., Dickman, R. L., and Clemens, D. P. 1986, *Ap. J.*, **309**, 619.
McDavid, D. 1984, *Ap. J.*, **284**, 141.
Moneti, A., Pipher, J. L., Helfer, H. L., McMillan, R. S., and Perry, M. L. 1984, *Ap. J.*, **282**, 508.
Myers, P. C., and Goodman, A. A. 1988*a*, *Ap. J. (Letters)*, **326**, L27.
———. 1988*b*, *Ap. J.*, **329**, 392.
Myers, P. C., Ho, P. T. P., Schneps, M. H., Chin, G., Pankonin, V., and Winnberg, A. 1978, *Ap. J.*, **220**, 864.
Purcell, E. M. 1979, *Ap. J.*, **231**, 404.
Seki, M. 1990, in *IAU Symposium 140, Galactic and Extragalactic Magnetic Fields*, ed. R. Beck, P. P. Kronberg, and R. Wielebinski (Dordrecht: Kluwer), in press.
Serkowski, K. 1974, *Methods Exper. Phys.*, **12**, Part A, 361.
Strom, K. M., Strom, S. E., Wolff, S. C., Morgan, J., and Wenz, M. 1986, *Ap. J. Suppl.*, **62**, 39.
Strom, S. E., Strom, K. M., and Edwards, S. 1988, in *Galactic and Extragalactic Star Formation*, ed. R. E. Pudritz and M. Fich (Dordrecht: Kluwer), p. 53.
Tamura, M., Nagata, T., Sato, S., and Tanaka, M. 1987, *M.N.R.A.S.*, **224**, 413.
Troland, T. H., and Heiles, C. 1986, *Ap. J.*, **301**, 339.
Turnshek, D. A., Turnshek, D. E., and Craine, E. R. 1980, *A.J.*, **85**, 1638 (TTC).
Ungerechts, H., and Thaddeus, P. 1987, *Ap. J. Suppl.*, **63**, 645.
Vrba, F. J., Coyne, G. V., and Tapia, S. 1981, *Ap. J.*, **243**, 489.
Vrba, F. J., Strom, S. E., and Strom, K. M. 1976, *A.J.*, **81**, 958.
———. 1988, *A.J.*, **96**, 680.
Wilking, B. A., Lebofsky, M. J., Rieke, G. H., and Kemp. J. C. 1979, *A.J.*, **84**, 199.

PIERRE BASTIEN and FRANÇOIS MÉNARD: Département de Physique, Université de Montréal, B.P. 6128, Succ. A. Montréal, Québec, Canada H3C 3J7

ALYSSA A. GOODMAN: Astronomy Department, University of California, Berkeley, CA 94720

PHILIP C. MYERS: Harvard-Smithsonian Center for Astrophysics, 60 Garden Street, Cambridge, MA 02138